AIAA JOURNAL
Vol. 37, No. 3, March 1999

Investigation of Unsteady Boundary Layer Developed on a Rotationally Oscillating Circular Cylinder

T. Lee*
McGill University, Montreal, Quebec H3A 2K6, Canada

The unsteady boundary layer developed on a rotationally oscillating circular cylinder was examined using closely spaced, multiple hot-film sensor (MHFS) arrays at selected forcing rotational oscillation frequencies ($S_f = f_o D/U_0 = 0.0064$–0.0217) and amplitudes ($\Delta\theta = \pm 27.7$ and ± 39.25 deg) for $Re < 5.6 \times 10^4$. Hot-wire cylinder wake characterizations and smoke-tunnel flow-pattern visualizations were also made to supplement the MHFS measurements. The results show that the spatiotemporal progression of the stagnation and upper and lower separation points and the state of the unsteady boundary layer developed on the oscillating cylinder can be identified both nonintrusively and simultaneously. The symmetry observed in the instantaneous locations of the upper and lower separation points, at small oscillation frequency, is consistent with the identical wake width found between the stationary and oscillating cylinders. The MHFS measurements also indicate a direct coupling between the dominant frequencies of flow oscillations at the leading-edge stagnation region, laminar-separation unsteadiness, and vortex shedding. The MHFS characterization of the unsteady boundary layer provides an increased understanding of unsteady flow phenomena, which are prerequisites for the control and management of unsteady separation over bluff bodies. However, higher forcing frequencies need to be investigated.

Nomenclature

D	= cylinder diameter
F_L	= lift produced by the induced circulation, $\rho\Gamma U_0$
f_{MHFS}	= vortex-shedding frequency extracted from multiple hot-film sensor (MHFS) signals
f_o	= oscillation frequency
f_S	= vortex-shedding frequency measured with a hot-wire probe
L	= length of the cylinder
R	= radius of the cylinder
Re	= Reynolds number, DU_0/ν
S	= sensor spacing
S_f	= forced Strouhal number, $f_o D/U_0$
Sr	= Strouhal number for fixed cylinders, $f_S D/U_0$ or $f_{\text{MHFS}} D/U_0$
t	= time
U_0	= freestream velocity
α	= spin ratio, $R\omega_0/U_0$
Γ	= induced circulation, $(\theta_{S1} + \theta_{S2})R\omega_0$
$\Delta\theta$	= oscillation amplitude
θ_{sep}	= mean separation point on a stationary circular cylinder
θ_{stg}	= stagnation point
θ_{S1}	= upper separation point
θ_{S2}	= lower separation point
$\theta(t)$	= instantaneous angular position, $\Delta\theta \sin 2\pi f_o t$
ν	= kinematic viscosity of fluid
ρ	= density of the fluid
τ	= ωt
$\omega_{\max}$	= maximum angular velocity of the cylinder rotation
ω_0	= angular velocity of the cylinder rotation
ω^*	= nondimensional oscillation amplitude, $R\omega_{\max}/U_0$

Introduction

THE flow past a circular cylinder is a classical problem that is of importance to both fundamental and applied fluid dynamists. The appearance of the vortex street in the wake of the cylinder produces the cyclic fluid forces acting on the cylinder. This interaction between the fluid and cylinder causes a flow-induced vibration when the vortex-shedding frequency is near the natural frequency of the cylinder. The vortex-shedding process has been studied by numerous workers since the latter half of the 19th century and still presents a challenge despite its apparent simplicity. A wealth of literature exists on this subject, as well as several review papers.[1–3] However, when the flow takes place in a fluid relative to a rotating cylinder, a new series of flow phenomena emerges.

Flow past a rotating circular cylinder is a prototyical problem in the study of unsteady flow separation. It is also of considerable practical importance in boundary-layer flow control.[4–6] Rotation of all or part of a body may also have applications in active or feedback control of vortex shedding, with important consequences for wake modification and the reduction of flow-induced vibration. The flow around a rotating or spinning circular cylinder has been studied rather extensively by researchers elsewhere.[7–17] Much effort has been made to investigate both numerically and experimentally the effects of the spin ratio α on the modification of the vortex wake and its associated characteristics, as well as the circulation-induced lift $F_L\,[=\rho\Gamma U_0$, where $\Gamma = (\theta_{S1} + \theta_{S2})R\omega_0$, and θ_{S1} and θ_{S2} are the upper and lower separation points with respect to the instantaneous front stagnation of the cylinder]. It was found that, depending on the magnitude of α, the front stagnation point θ_{stg} and θ_{S1} and θ_{S2} could move greatly from their original positions of the nonrotating case and that the vortex formation process could be greatly suppressed or even eliminated. However, only a comparatively smaller number of researchers have investigated the effects of rotational oscillation of the cylinder.[18–25]

The effects of rotary oscillations on the cylinder wake were first studied by Okajima et al.[18] They examined the forces acting on a rotationally oscillating cylinder with a nondimensional peak rotation rate ω^* of 0.2–1.0 and a forcing Strouhal number S_f ranging from 0.05 to 0.3, and they observed a synchronization similar to that observed for a cylinder in transverse and in-line oscillation.[26–28] Later, Taneda[19] studied the effects of rotational oscillation at $Re = 3 \times 10$–10^2 and indicated that, at very high oscillating frequencies and amplitudes ($\omega^* > 7$–27), the vortex-shedding process could be nearly eliminated. Recently, Filler et al.[21] have studied experimentally the frequency response of the shear layers separating from a circular cylinder subjected to small-amplitude rotational oscillations for $Re = 2.5 \times 10^2$–1.2×10^3. Filler et al. observed that rotational oscillations corresponding to cylinder peripheral speeds less than 3% of the freestream can influence the Kármán mode of vortex generation.

Received Jan. 13, 1998; revision received Aug. 3, 1998; accepted for publication Sept. 15, 1998.

*Assistant Professor, Department of Mechanical Engineering.

On the other hand, Tokumaru and Dimotakis[22,23] have shown that rotational oscillation at very large amplitudes can suppress the vortex shedding and produce significant reduction in drag on the cylinder, based on the flow visualization and velocity measurement in the cylinder wake. It is now clear that, depending on the frequency and amplitude of oscillation, the wake could become wider, narrower, or remain the same and that any major change in the Strouhal frequency $Sr\ (= f_S D/U_0$, where f_S is the frequency of vortex shedding behind a stationary cylinder) has to be accomplished by a change in the flow separation (θ_{S1} and θ_{S2}) and the associated wake width by the forced Strouhal frequency S_f and the oscillation amplitude ω^*. Accurate measurements of the instantaneous locations of the stagnation and the upper and lower separation points are, therefore, critical in better understanding the coupling between body motion and Kármán vortex shedding that is taking place mainly through the effect of body motion on the temporal development of the unsteady boundary layer between stagnation and flow separation points. However, the identification of the stagnation and separation points on a rotating cylinder in a crossflow has relied heavily on the qualitative interpretation of flow visualization, and experimental techniques capable of characterizing the spatiotemporal progression of the stagnation and separation points and the state of the unsteady boundary-layer flow across the regions of interest quantitatively are greatly needed.

The purpose of this study was to investigate nonintrusively the unsteady boundary layer developed on a rotationally oscillating circular cylinder using closely spaced, multiple hot-film sensor (MHFS) arrays. Hot-wire cylinder wake profile and vortex-shedding frequency measurements, as well as smoke-tunnel flow-pattern visualizations, were also made to supplement the hot-film sensor measurements. Special emphasis was placed on the structurally nonintrusive measurement of the spatiotemporal progression of the stagnation and the upper and lower separation points on the oscillating cylinder at small oscillation frequencies and amplitudes. It is anticipated that the present nonintrusive MHFS characterization of the unsteady boundary layer would provide an increased understanding of unsteady flow phenomena, which are prerequisites for the control and management of unsteady separation over aerodynamic or bluff-body objects.

Experimental Methods and Procedures

Flow and Test Facilities

The experiment was performed in the $2 \times 3 \times 6\ \text{ft}^3$ low-speed wind tunnel in the Aerodynamics Laboratory in the Department of Mechanical Engineering of McGill University. The freestream turbulence intensity was 0.27% at $U_0 = 13.9$ m/s, and the flow nonuniformity was less than 1%. A smooth, hollow aluminum circular cylinder (with $D = 6.25$ cm and $L/D = 14$) mounted horizontally in the center of the test section was used in the present investigation (Fig. 1). Circular disks of 18-cm diameter with sharp leading edges were attached to both ends of the cylinder to keep the two dimensionality of the flow. The end-disk design and the aspect ratio used in this experiment followed dimensions used by Lee and Budwig.[29] The cylinder was supported in bearings attached to the tunnel walls, with one end of the cylinder protruding through the tunnel wall and connected to a stepping motor so that it could be rotated sinusoidally [$\theta(t) = \Delta\theta \sin 2\pi f_o t$] at selected oscillating frequencies (f_o or S_f) and amplitudes ($\Delta\theta$ or ω^*). The computer control algorithm generated independent, preprogrammed pulse trains that determined the driving stepper motor shaft displacement and rate histories. The resulting cylinder motion was motored using a TRW-type DP801 potentiometer (with an accuracy of ± 0.5 deg) mounted at the other end of the cylinder. Figure 2 shows the typical sinusoidal oscillation waveforms. For the oscillating cylinder experiment, the oscillation frequencies and amplitudes tested were $f_o = 1.4$–2.8 Hz ($S_f = 0.0064$–0.0217) and $\Delta\theta = \pm 27.7$ and ± 39.25 deg, respectively, with $Re = 3.4 \times 10^4$–5.6×10^4. The low oscillation frequencies used were due to the limitation of the present experimental

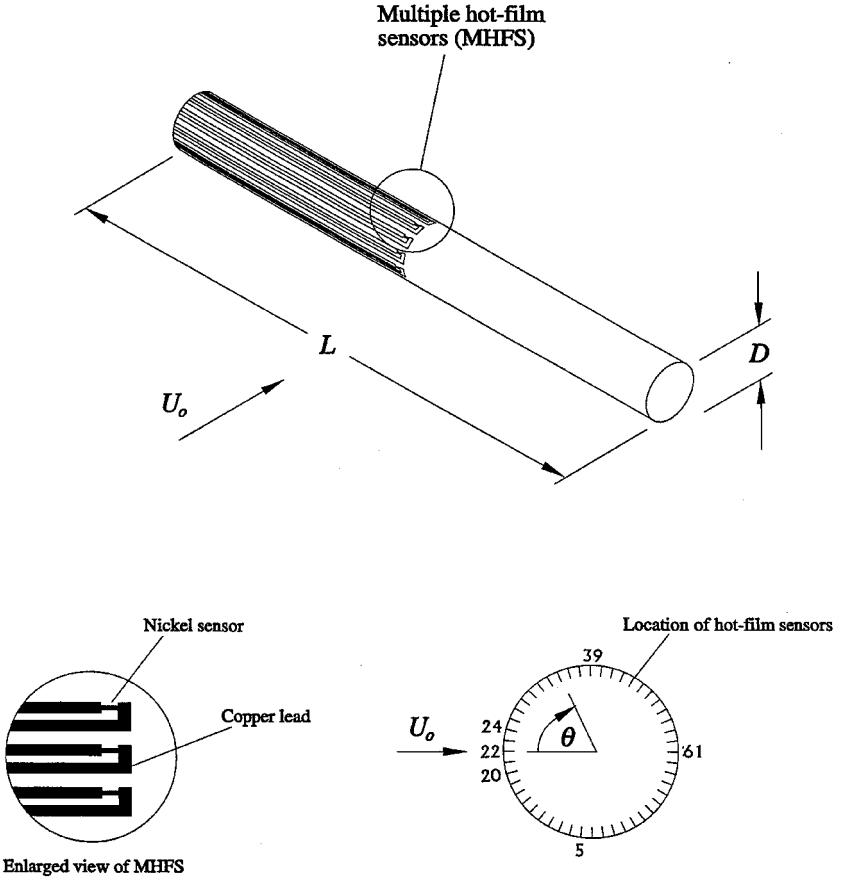

Fig. 1 Schematics of the MHFS pattern and the layout of the copper leads on the cylinder model.

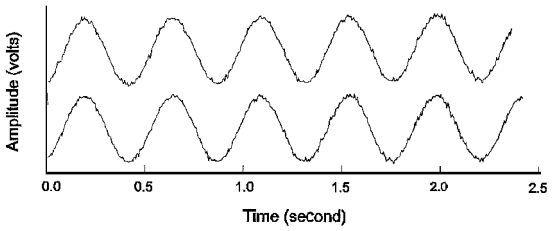

Fig. 2 Typical sinusoidal oscillation waveforms: upper trace, cylinder angular position from the output of a potentiometer, and lower trace, reference signal from a function generator.

setup. Note that much larger magnitudes of S_f (such that ω^* would be comparable with U_0) would be necessary to send the vorticity stored in the boundary layer into the wake in a regular manner.[22,23] However, due to the limitation of the present experimental setup, small values of S_f were used to identify the spatiotemporal movement of θ_{stg}, θ_{S1}, and θ_{S2} on a rotationally oscillating cylinder instead of investigating the effects of the rotation on characteristic parameters of the flowfield.

The wake of the cylinder was measured by a hot-wire probe (DISA P11) with a Dantec 56C17 constant-temperature anemometer (CTA). The overheat ratio was set at 1.8. The hot-wire probe was mounted on a sting extended from a computer-controlled, two-dimensional traversing mechanism. The probe was moved with accuracy in the x and y directions with 20 and 25 μm, respectively. All hot-wire calibrations, mean-flow measurements, freestream turbulence levels, rms disturbances measurements, and subsequent processing were performed on a 486 personal computer with a 12-bit A/D converter board (Computer Boards Model Das16/330), using the Streamer data acquisition software. The hot-wire signals were sampled at 2 kHz with a cutoff of 250 Hz. Waveforms and frequency spectra of streamwise velocity fluctuations were also recorded and analyzed using a dual-channel fast Fourier transform spectrum analyzer (Hewlett Packard Model 3562A). For vortex-shedding frequency measurement, the hot-wire probe was located $2D$ downstream of the center and $1D$ away from the axis of the cylinder.

The spanwise flow structures around the cylinder were visualized by using a smoke tunnel at a flow speed of about 6 m/s, which renders $Re = 2.458 \times 10^4$. A similar oscillation mechanism was also built so as to reproduce the harmonic motion imposed on the circular cylinder in the smoke tunnel. The visualized wake structures at different instantaneous rotation angles were recorded with a 60-Hz video camera together with a 35-mm still camera using Kodak ASA 1600 color film and a shutter speed of $\frac{1}{500}$ s. The oscillation frequency was fixed at 2.8 Hz ($S_f = 0.0217$).

MHFS Arrays

The MHFS arrays used in the present experiment consist of a number of thin nickel films (0.2 μm), which are electron-beam evaporated onto a thin polyimide substrate (50 μm) in a straight-line array. Each sensor consists of a nickel film 2 mm long and 100 μm wide with 8-μm, copper-coated nickel leads routed to provide wire attachment away from the measurement location. The nominal resistance of the sensor is 7.0 Ω. The entire sensor array consists of 78 sensors spaced at $S = 2.5$ mm apart (which renders an angular spacing of 4.615 deg) with sensor S_{22} located at the front stagnation point (FSP) of the cylinder ($\theta = 0$ deg). The sensor number indicates the location of the hot-film sensors along the surface of the cylinder and is proportional to the distance covered along the upper (S_{22}–S_{61} covering $\theta = 0$–180 deg) and lower (sensors S_{61}–S_{21} covering $\theta = -180$ to -4.615 deg) surfaces of the cylinder from the FSP. The sensor array was bonded onto the entire cylinder surface using double-sided Mylar® adhesive tape, which prevented the sensor array from introducing surface irregularities to the model surface. Figure 1 shows the schematics of the MHFS pattern and the layout of the copper leads on the cylinder model.

Groups of 18 of the 78 sensors were systematically connected to 18 CTAs (AA Laboratory Model AN-1003) to obtain the time history and spectral information at each sensor position. The sensors were connected to the CTAs using a combination of magnet wire and a BNC coaxial cable to minimize the disturbance to the flow in the tunnel test section. The overheat ratio was set at 1.10, which ensured that only a small amount of heat was introduced and the heated thin films caused little disturbance to the shear layer or to each other. This was checked by heating the films individually and in groups while monitoring the effects on other films. CTA output signals were low-pass filtered (with a cutoff of 500 Hz) and amplified by a gain between 10 and 50. The sensors were uncalibrated, and the overheat and offset voltages for each sensor were carefully adjusted such that each sensor was at nearly the same operating conditions. The fluctuating voltage output of the CTA represents a function of the dynamic shear stress present at each hot-film sensor location. Separation is indicated by a low level of average heat transfer. Furthermore, the influence of nonnegligible heat transfer through polyimide substrate to the model and the fluid, which had been found to be significant in quantitative measurements in air flow,[30,31] was not believed to be a problem in the present method. For each set of data, 18 CTA channels from the MHFS and one CTA channel from the hot-wire probe were simultaneously sampled and digitized at 2 kHz per channel by the data acquisition system described in the "Flow and Test Facilities" section. The output signal from the potentiometer was also sampled and serves as the reference signal between each set of CTA outputs. The amplified signals were also connected to a four-channel oscilloscope (LeCroy Model 9304) to provide on-line time history traces of the operating group of sensors. No calibration of the MHFS was performed as the objective of this experiment was to document the qualitative behavior of the boundary-layer shear stress characteristics. Therefore, the heat transfer or the voltage output level of the heated hot-film sensor gives a direct recognition of the state of the boundary layer over it. The laminar and transitional flows are indicated by a low heat transfer and a rapid rise in heat transfer, respectively.

Results and Discussion

Stationary Cylinder

To facilitate the understanding of the unsteady effects on the boundary layer developed on a rotationally oscillating cylinder, the locations of the stagnation and separation points and the state of the boundary layer developed on a stationary circular cylinder were examined first. Figures 3a and 3b show the typical composite plot of the simultaneously acquired MHFS outputs from a stationary circular cylinder with $Re = 5.6945 \times 10^4$. The numbers shown on the right (left) ordinate axes in Fig. 3 correspond to sensor numbers (angular positions) on the cylinder model. The y axis also represents the voltage output level of each sensor. The outputs were self-scaled to a peak-to-peak value of one; this allows the regions of change to be easily identified and provides a clear qualitative picture. The lowermost curve represents the time traces obtained with a hot-wire probe positioned in the wake of the cylinder.

Figure 3a shows the selected time histories of MHFS outputs (S_{14}–S_{61} covering $\theta = -36.92$ to $+180$ deg), which illustrate the direct recognition of the locations of the FSP and the boundary-layer separation point, as well as the state of the boundary layer developed on the stationary cylinder. Figure 3a indicates that, even in a visual comparison of the raw signals, there is a 180-deg phase shift (due to the presence of flow bifurcation at the stagnation point observed by Stack et al.[32]) between S_{21} and S_{23} ($\theta = -4.615$ and $+4.615$ deg), which allows the identification of the FSP at S_{22} ($\theta_{stg} = 0$ deg). Also, because at the point of separation the dividing streamline emanates from the body, a separation point at around S_{39}, i.e., a mean separation angle θ_{sep} of about 78.5 deg, could also be recognized based on the presence of the 180-deg out-of-phase phenomenon between the outputs of S_{38} and S_{39} ($\theta = 73.84$ and 78.455 deg). The 180-deg phase-shift phenomenon also indicates the presence of the first harmonics at S_{21} and S_{39} and can be interpreted as follows: The shear layer between the separation region and the freestream flow is unstable to Helmholtz instabilities. These instabilities grow noticeably and result in transverse oscillations of the separating streamline. If these oscillations are small enough, then the flowfield in the vicinity of the separation point can be decomposed into the mean flow and the small variations, due to the moving separating streamlines. The mean shear stresses upstream and downstream of the separation point are directed in the upstream and downstream directions,

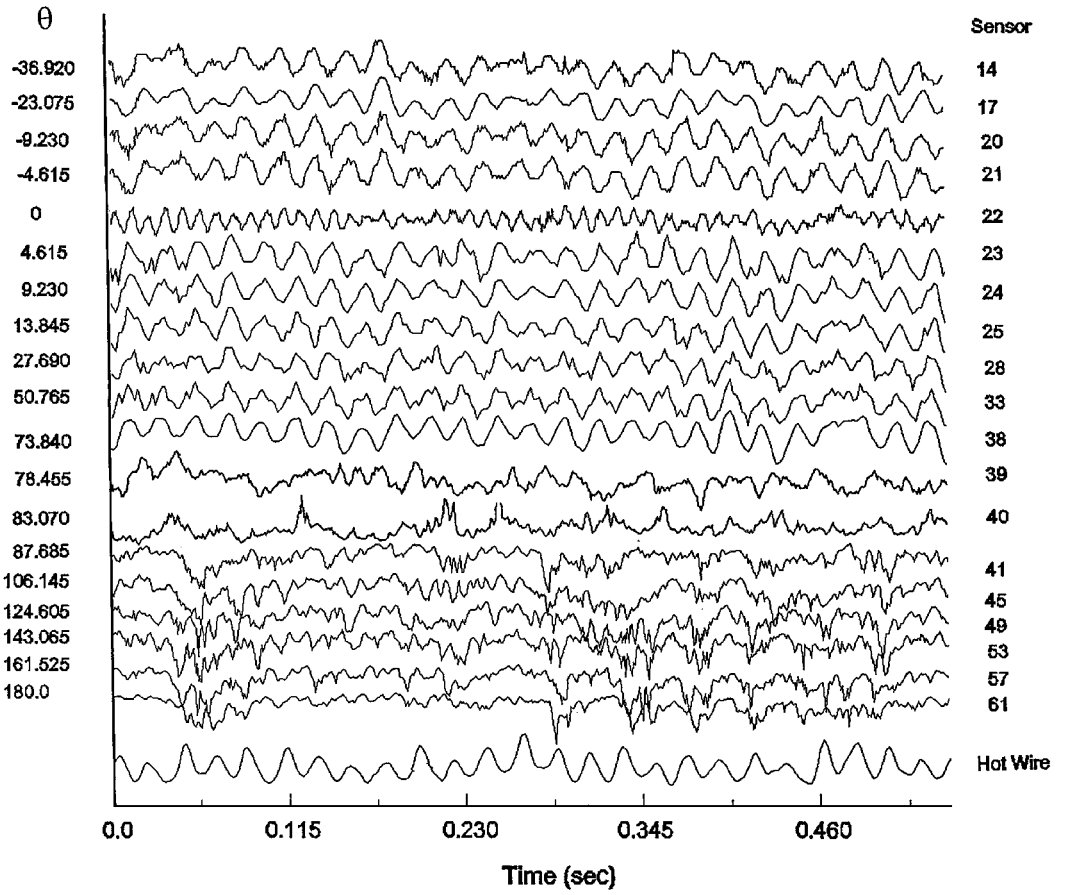

a) Time traces

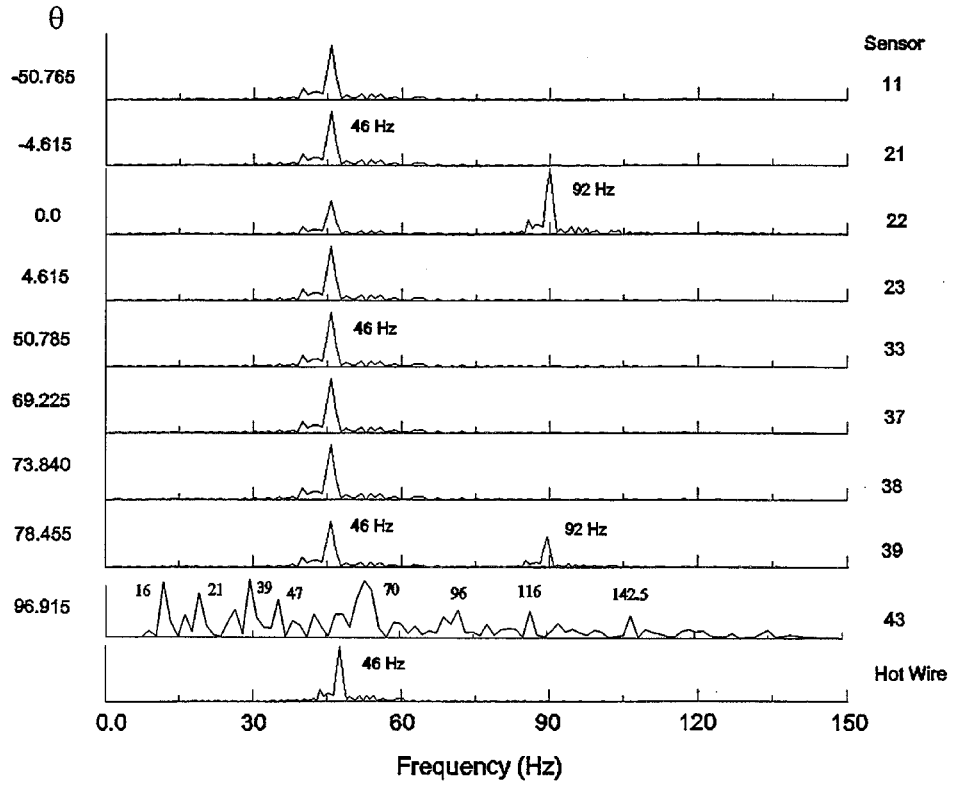

b) Spectral contents

Fig. 3 Composite plots of selected MHFS outputs and a hot-wire probe for a stationary cylinder with $Re = 5.6945 \times 10^4$.

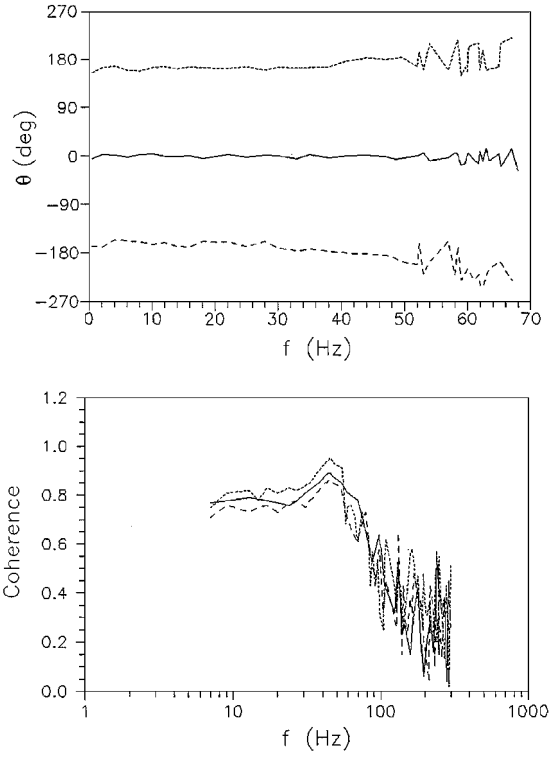

Fig. 4 Phase angles and coherence across selected MHFS outputs shown in Fig. 3a: a) phase angles: ——, in phase (across S_{23} and S_{33}); · · · ·, +180 deg out of phase (across S_{21} and S_{23}); and - - - -, −180 deg out of phase (across S_{38} and S_{39}); and b) coherence: · · · ·, across S_{21} and S_{23}; - - - -, across S_{38} and S_{39}; and ——, across S_{39} and the hot wire.

respectively, which leads to the observed 180-deg out-of-phase phenomenon in the hot-film output signals. The existence of the 180-deg phase shift can also be confirmed from the phase angles and the coherence obtained by cross correlating the simultaneously recorded MHFS outputs across the points of interest (Fig. 4).

Figure 3b shows the corresponding spectral contents of the selected MHFS output signals shown in Fig. 3a. The frequency in hertz is plotted on the x axis, and the power spectral plots have arbitrary y-axis scales. A linear scale was used to concentrate on the low-frequency end of the spectra. The results reveal that the dominant characteristic oscillation frequency f_{MHFS} (measured by MHFS) of 46 Hz of the boundary layer flow is identical to the frequency of the vortex shedding f_S (measured by a hot wire positioned in the cylinder wake). Also, the presence of the first harmonics (92 Hz) in the power spectrum of signals from sensors S_{22} and S_{39} suggests that the stagnation and separation points were fluctuating across sensors S_{22} and S_{39}, respectively. The presence of a strong double peak whenever the stagnation or separation point passed over a sensor or gauge twice during a cycle was also observed by Dwyer and McCroskey.[33] A mean Strouhal number $Sr\,(=f_S D/U_0 = f_{\mathrm{MHFS}} D/U_0)$ of 0.208 was found for $Re = 2.6 \times 10^4$–6.8×10^4 for a single stationary circular cylinder (Table 1), compared with the empirical value of 0.21 obtained by Roshko.[34]

Figures 4a and 4b show the phase relations and coherence obtained by cross correlating the simultaneously obtained MHFS signals across points of interest. For comparison, the phase relations between pairs of signals from hot-film sensors located on either side of the stagnation point are shown in Fig. 4a (solid line), which clearly indicates that there is zero phase difference between them (S_{21}–S_{33}). The stagnation point was recognized by the presence of a +180-deg phase difference between sensors S_{21} and S_{23} (dotted line). The separation point was identified by the presence of a −180-deg phase difference between sensors S_{38} and S_{39} (dashed line). Figure 4b reveals that the coherence between S_{21} and S_{23} (dotted line) and S_{38} and S_{39} (dashed line) was also a maximum at the dominant oscillation frequency (46 Hz) of the boundary layer. Furthermore, the hot-wire signals in the wake region have good coherence with the outputs of S_{39} (solid line). Figure 4 not only confirms the presence of laminar separation between sensors S_{38} and S_{39} but also suggests that the laminar separation was unsteady, with a characteristic frequency of 46 Hz.

Table 1 Stationary circular cylinder measure with a hot-wire probe and MHFS at different Reynolds numbers, f_S, f_{MHFS}, and Sr

$Re, \times 10^4$	f_S	f_{MHFS}	Sr
2.687	21.3	21.3	0.206
3.108	24.7	24.7	0.207
3.605	28.6	28.6	0.206
3.9	30.9	30.9	0.206
4.35	34.8	34.8	0.208
4.865	38.5	38.5	0.206
5.6945	46	46	0.2107
6.2450	49.7	49.7	0.207
6.7980	54	54	0.2068

Figures 3 and 4 indicate the following: 1) The time traces of the MHFS (S_{21}–S_{14} and S_{23}–S_{38}) are in phase on each side of the stagnation point (S_{22}). 2) Compared to signals from S_{21}–S_{38}, signals from S_{40} exhibit an increase in amplitude and a loss in periodicity (due to the small, random backflow immediately downstream of laminar separation). 3) The frequency of the vortex shedding can be extracted directly from MHFS output signals (because the cylinder boundary layer reacts in response to vortex shedding, which is the result of a global absolute instability of the near wake region). 4) There is an appearance of the first harmonics (92 Hz) at S_{22} and S_{39}. 5) The MHFS measurements also indicate a direct coupling between the dominant frequencies of flow oscillations at the leading-edge stagnation region, laminar-separation unsteadiness, and vortex shedding. In summary, the structurally nonintrusive MHFS measurements of the stagnation and separation points and the behavior of the boundary layer are useful in the characterization of the boundary layer developed on a cylinder (especially in a group of circular cylinders), as well as in the study of unsteady separated flows. The extraction of the characteristics of the boundary layer (through a qualitative way) also relieves the great difficulty encountered in the calibrating of multiple surface-mounted hot-film sensors. These difficulties are attributed to the need to 1) calibrate all hot-film sensors in a reference unsteady flow before installation, 2) provide a reference flow at each sensor, or 3) calibrate the sensors by comparison to a traceable and portable reference probe.[35] Furthermore, note that interpretation of hot-film signals is more straightforward for periodic unsteady flows because the changes from one flow state to another can be more readily identified (as shown in Fig. 5) than the characteristics of a steady-state flow.

Rotating Cylinder

Figures 5a and 5b show the time histories of MHFS outputs on a rotationally oscillating cylinder with $f_o = 1.4$ Hz ($S_f = 0.0064$), $\Delta\theta = \pm 39.25$ deg, and $Re = 5.6945 \times 10^4$. The lowermost curve represents the variation in the potentiometer voltage, which indicates the angular location of a reference sensor on the model at a given instant. The angular velocity of cylinder rotation follows a sine wave, where the positive angular velocity corresponds to a counterclockwise rotation of the cylinder set in a flow geometry as shown in Fig. 2. The time trace right above the potentiometer output was obtained with a hot-wire probe positioned in the wake of the cylinder. The y axis represents the voltage output level of each sensor. The repeatability from cycle to cycle was found to be extremely good, and for clarity only two cycles needed to be shown.

Figure 5a shows that, because the convective heat transfer at the stagnation point is a minimum, the movement of the FSP with $\tau = \omega t$ (indicated by the locus of FSP) is clearly indicated by the travel of the minimum voltages from outputs of S_{22}–S_{39} during one cycle of oscillation. Sensor S_{22} at time instant T_1 traversed the instantaneous FSP first, followed by sensors S_{23}–S_{39} (at T_2–T_{18}) during downstream (counterclockwise) motion, then reversed direction, followed

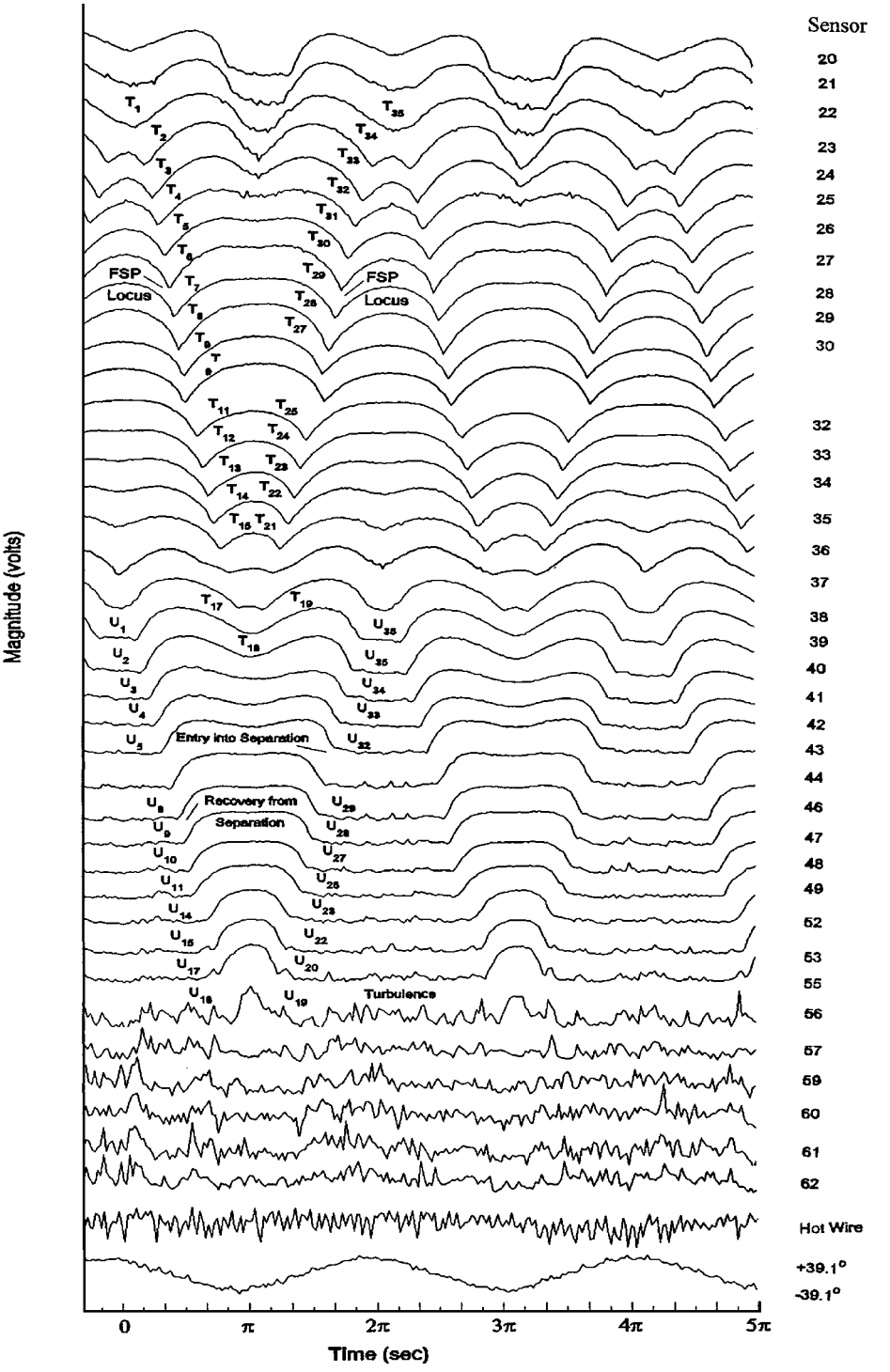

a) S_{20}–S_{62}

Fig. 5 Composite plots of selected MHFS outputs and a hot-wire probe for a rotationally oscillating cylinder with f_o = 1.4 Hz, $\Delta\theta = \pm$ 39.25 deg, and $Re = 5.6945 \times 10^4$.

by sensors S_{39}–S_{22} (at T_{18}–T_{35}) during upstream (clockwise) motion. The spatiotemporal progression of the FSP with time for $f_o = 1.4$ Hz and $\Delta\theta = \pm 27.7$ and ± 39.25 deg is summarized in Fig. 6 (indicated by cross and diamond symbols, respectively). The nonintrusive and simultaneous identification of the movement of the instantaneous location of the FSP on the surface of the cylinder is important in the determination of the corresponding magnitudes of the upper and lower separation on the surface of the sinusoidally oscillated circular cylinder.

Figure 5a also shows that the boundary-layer flow separation is indicated by the second minimum in the MHFS voltage outputs, with laminar signals on one side and turbulent signals on the other. The flow separation is also associated with rapid transition to turbulence immediately downstream of the separation points (especially at sensor S_{56}). The spatiotemporal progression of the upper separation point θ_{S1} is indicated by the lines of entry into separation (S_{38}–S_{56}) and recovery from separation (S_{56}–S_{38}) at time instants U_1–U_{36}. Similarly, the spatiotemporal progression of the

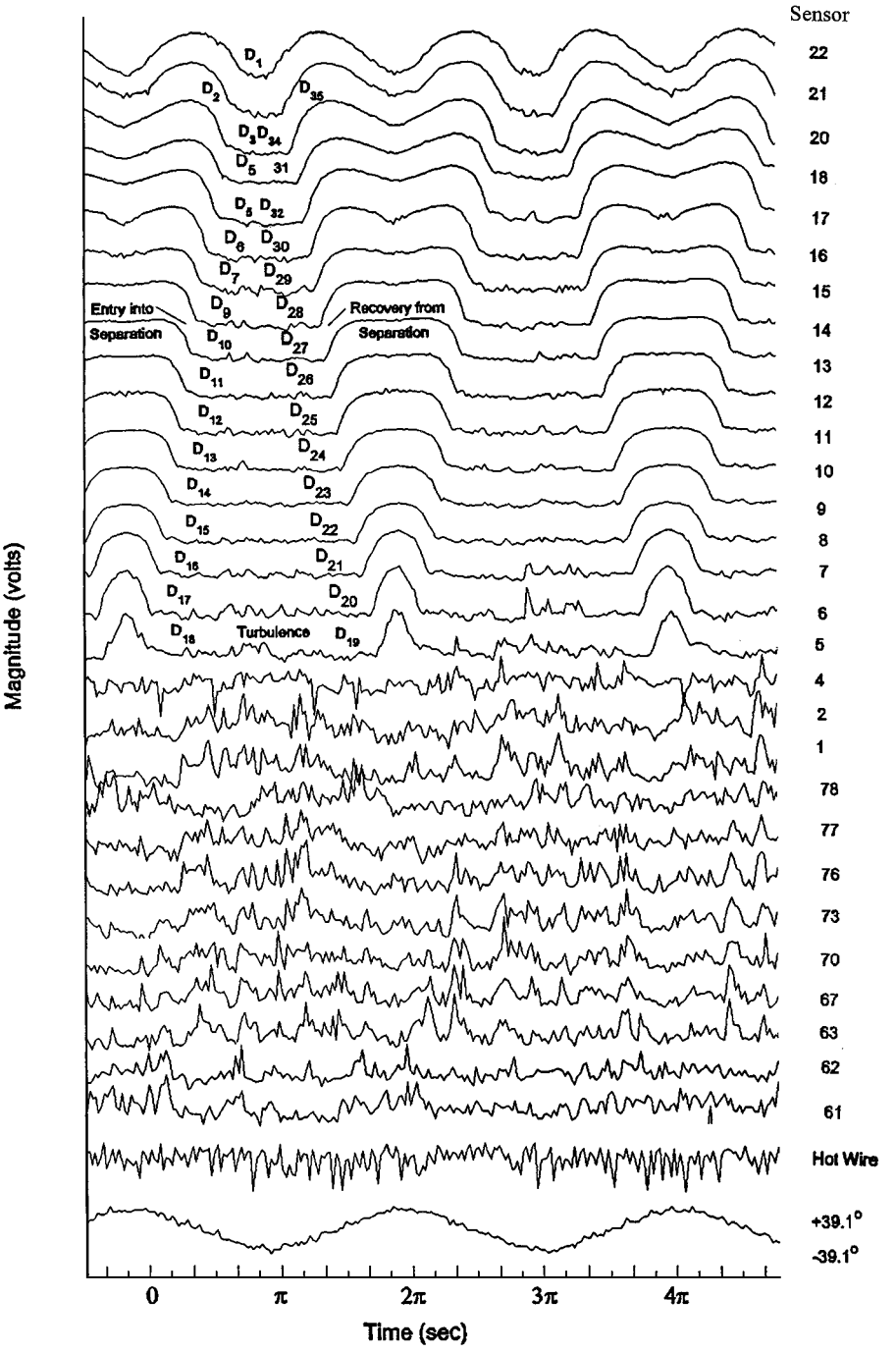

b) S_{22}–S_{61}

Fig. 5 (Continued)

lower separation point θ_{S2} could also be recognized and indicated by the lines of entry into separation (S_{22}–S_5) and recovery from separation (S_5–S_{22}) at time instants D_1–D_{35} (Fig. 5b). Figures 5a and 5b indicate that, during clockwise or downstream motion, the entry separation θ_{S1} of sensors S_{38}–S_{56} was accompanied by the recovery from separation θ_{S2} of sensors S_{22}–S_5 and vice versa. The variation of θ_{S1} and θ_{S2} with $f_o = 1.4$ Hz and $\Delta\theta = \pm 27.7$ and ± 39.25 deg for $Re = 5.6945 \times 10^4$ is summarized in Fig. 6.

Figure 6 shows that, for small values of oscillation frequency ($S_f \leq 0.0217$), 1) a symmetry is always present for upper and lower separation points during clockwise and anticlockwise rotation of the cylinder, 2) the instantaneous values of θ_{S1} and θ_{S2} can be obtained from the numbers of sensors located between the locus of FSP and lines of entry into separation, and 3) θ_{S1} and θ_{S2} are identical to θ_{sep}, which indicates that the small moving-wall and accelerated flow effects have no noticeable influence on the behavior of the unsteady boundary layer. Experimental apparatus capable of oscillating the cylinder at frequencies comparable to the frequency of the vortex shedding is greatly needed to document the effects of the oscillation motion of the cylinder on the delay and promotion of the separation points and the temporal development of the unsteady boundary layer, as well as the possible suppression of the vortex wake (which is of great interest in view of the investigations of flow past rotating circular cylinders). The symmetry in the instantaneous locations of the FSP and the upper and lower separation points for small values of S_f (≤ 0.0217) observed in Figs. 5 and 6

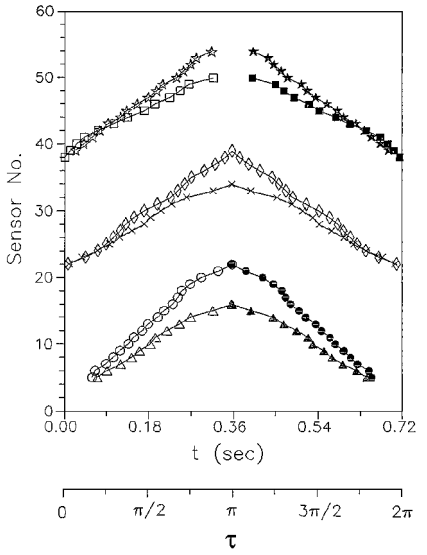

Fig. 6 Variation of the front stagnation point and the upper and lower separation points with $\Delta\theta$ for $f_o = 1.4$ Hz and $Re = 5.6945 \times 10^4$; stagnation point: ×, $\Delta\theta = 55.4$ deg, and ◇, $\Delta\theta = \pm 39.25$ deg; entry into θ_{S1}: ®, $\Delta\theta = \pm 27.7$ deg, and ★, $\Delta\theta = \pm 39.25$ deg; recovery from θ_{S1}: □, $\Delta\theta = \pm 27.7$ deg, and ☆, $\Delta\theta = \pm 39.25$ deg; entry into θ_{S2}: △, $\Delta\theta = \pm 27.7$ deg, and ○, $\Delta\theta = \pm 39.25$ deg; recovery from θ_{S2}: ▲, $\Delta\theta = \pm 27.7$ deg, and ●, $\Delta\theta = \pm 39.25$ deg.

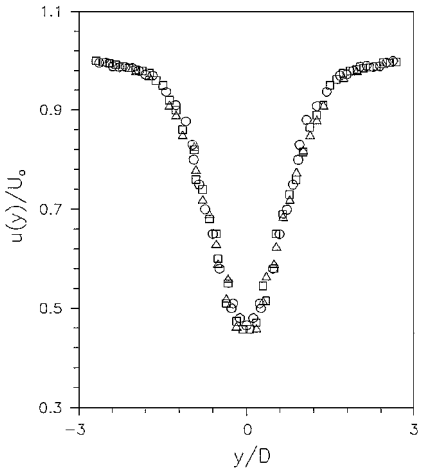

Fig. 7 Cylinder wake mean velocity profiles: ○, stationary cylinder; □, oscillating cylinder, $f_o = 1.4$ Hz ($S_f = 0.0064$) and $\Delta\theta = \pm 39.25$ deg; △, $f_o = 2.8$ Hz ($S_f = 0.0217$) and $\Delta\theta = \pm 27.7$ deg. The hot-wire probe was located four diameters downstream of the cylinder axis.

was further confirmed by the hot-wire wake profile measurements (Fig. 7), as well as by the smoke-tunnel, flow-pattern visualization results (not shown here). Both the measured wake widths (Fig. 7) and the visualized wake patterns (Fig. 8) reveal that the wake width behind an oscillating circular cylinder remained the same compared to that of a stationary cylinder (open circles), which again indicates that the small oscillation frequency has no observable influence on the characteristics of the cylinder wake as well as the magnitudes of θ_{stg}, θ_{S1}, and θ_{S2}. As shown by smoke-tunnel flow visualization for $Re = 2.4580 \times 10^4$ (Fig. 8), the vortex wake generated behind a circular cylinder oscillated rotationally at $f_o = 2.8$ Hz and $\Delta\theta = \pm 39.25$ deg (Fig. 8b), which is qualitatively similar to those observed in a stationary cylinder wake (Fig. 8a). Figure 8 together with Figs. 6 and 7 further demonstrates that higher values of S_f and $\Delta\theta$, especially S_f, are needed to have noticeable effects on the overall narrowing or widening of the wake, as well as the formation of distinct vortical structures in the wake.

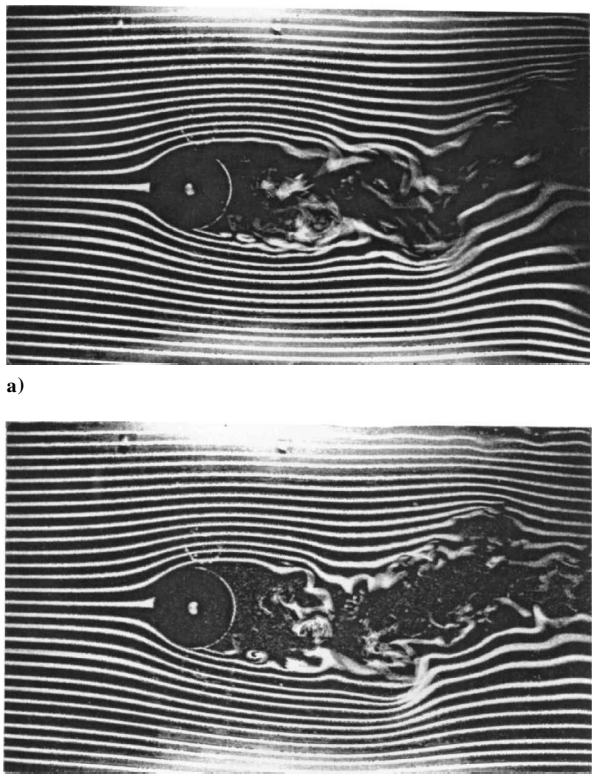

a)

b)

Fig. 8 Smoke-tunnel flow visualization for $Re = 2.4580 \times 10^4$, with the cylinder at its maximum clockwise position: a) stationary cylinder and b) rotationally oscillating cylinder with $f_o = 2.8$ Hz and $\Delta\theta = \pm 39.25$ deg.

Conclusions

The spatiotemporal progression of the front stagnation and separation points and the state of the boundary layers developed on a stationary and a rotationally oscillating circular cylinder were measured successfully using an MHFS array. The results show that there is a direct coupling between the dominant frequencies of flow oscillations at the leading-edge stagnation region, laminar-separation unsteadiness, and vortex shedding and that the frequency of the vortex shedding can be extracted directly using the MHFS array. It was also observed that, for small oscillation frequencies ($S_f \leq 0.0217$), a symmetry is always present for upper and lower separation points during clockwise and anticlockwise rotation of the cylinder and that the frequency of the vortex shedding and the wake width remain the same compared to those of a stationary circular cylinder. The MHFS characterization of the unsteady boundary layer will provide an increased understanding of unsteady flow phenomena, which are prerequisites for the control and management of unsteady separation over bluff bodies.

Acknowledgments

This work was supported by the Natural Sciences and Engineering Research Council of Canada. A. Woods is thanked for her help with the flow-visualization experiment.

References

[1]Berger, E., and Wille, R., "Periodic Flow Phenomena," *Annual Review of Fluid Mechanics*, Vol. 4, 1972, pp. 313–340.

[2]Bearman, P. W., "Vortex Shedding from Oscillating Bluff Bodies," *Annual Review of Fluid Mechanics*, Vol. 16, 1984, pp. 195–222.

[3]Griffin, O. M., and Hall, M. S., "Review: Vortex Shedding Lock-On and Flow Control in Bluff Body Wakes," *Journal of Fluids Engineering*, Vol. 113, No. 4, 1991, pp. 526–537.

[4]Schlichting, H., *Boundary Layer Theory*, McGraw–Hill, New York, 1979.

[5]Modi, V. J., Mokhtarian, F., and Yokomizo, T., "Effect of Moving Surfaces on the Airfoil Boundary-Layer Control," *Journal of Aircraft*, Vol. 27, No. 1, 1990, pp. 42–50.

[6]Tennant, J. S., Johnson, W. S., and Krothapalli, A., "Rotating Cylinder for Circulation Control on an Airfoil," *Journal of Hydronautics*, Vol. 10, No. 3, 1976, pp. 102–105.

[7]Glauert, M. B., "The Flow Past a Rapidly Rotating Circular Cylinder," *Proceedings of the Royal Society of London Series A: Mathematical and Physical Sciences*, Vol. 242, 1957, pp. 108–115.

[8]Swanson, W. M., "The Magnus Effect: A Summary of Investigations to Date," *Journal of Basic Engineering*, Vol. 83, No. 3, 1961, pp. 461–470.

[9]Ingham, D. B., "Steady Flow Past a Rotating Cylinder," *Computers and Fluids*, Vol. 11, No. 4, 1983, pp. 351–366.

[10]Diaz, F., Gavalda, J., Kawall, J. G., Keffer, J. F., and Giralt, F., "Vortex Shedding from a Spinning Cylinder," *Physics of Fluids*, Vol. 26, No. 12, 1983, pp. 3454–3460.

[11]Diaz, F., Gavalda, J., Kawall, J. G., Keffer, J. F., and Giralt, F., "Asymmetrical Wake Generated by a Spinning Cylinder," *AIAA Journal*, Vol. 23, No. 1, 1985, pp. 49–54.

[12]Coutanceau, M., and Menard, C., "Influence of Rotation on the Near-Wake Development Behind an Impulsively Started Circular Cylinder," *Journal of Fluid Mechanics*, Vol. 158, 1985, pp. 399–446.

[13]Aldoss, T. K., and Mansour, A., "Theoretical Calculations of the Flow Around a Rotating Circular Cylinder Placed in a Uniform Flow," *Journal of Fluids Engineering*, Vol. 110, No. 1, 1988, pp. 96–98.

[14]Badr, H. M., Coutaneau, M., Dennis, S., and Menard, C., "Unsteady Flow Past a Rotating Circular Cylinder at Reynolds Numbers 103 and 104," *Journal of Fluid Mechanics*, Vol. 220, 1990, pp. 459–484.

[15]Kimura, T., Tsutahara, M., and Wang, Z., "Wake of a Rotating Circular Cylinder," *AIAA Journal*, Vol. 30, No. 2, 1992, pp. 555, 556.

[16]Chang, C.-C., and Chen, R.-L., "Vortex Shedding from an Impulsively Started Rotating and Translating Cylinder," *Journal of Fluid Mechanics*, Vol. 235, 1992, pp. 265–298.

[17]Chen, Y.-M., Ou, Y.-R., and Pearlstein, A. J., "Development of the Wake Behind a Circular Cylinder Impulsively Started into Rotary and Rectilinear Motion," *Journal of Fluid Mechanics*, Vol. 253, 1993, pp. 449–484.

[18]Okajima, A., Takata, H., and Asanuma, T., "Viscous Flow Around a Rotationally Oscillating Circular Cylinder," Inst. of Space and Aeronautical Science, Rept. 532, Univ. of Tokoyo, Tokoyo, Japan, 1975, pp. 311–338.

[19]Taneda, S., "Visual Observations of the Flow Past a Circular Cylinder Performing a Rotary Oscillation," *Journal of the Physical Society of Japan*, Vol. 45, 1978, pp. 1038–1043.

[20]Wu, J., Mo, J., and Vakili, A., "On the Wake of a Cylinder with Rotational Oscillations," AIAA Paper 89-1024, 1989.

[21]Filler, J. R., Marston, P. L., and Mih, W. C., "Response of the Shear Layers Separating from a Circular Cylinder to Small-Amplitude Rotational Oscillation," *Journal of Fluid Mechanics*, Vol. 231, 1991, pp. 481–499.

[22]Tokumaru, P. T., and Dimotakis, P. E., "Rotary Oscillation Control of a Cylinder Wake," *Journal of Fluid Mechanics*, Vol. 224, 1991, pp. 77–90.

[23]Tokumaru, P. T., and Dimotakis, P. E., "The Lift of a Cylinder Executing Rotary Motions in a Uniform Flow," *Journal of Fluid Mechanics*, Vol. 255, 1993, pp. 1–10.

[24]Lu, X.-Y., and Sato, J., "A Numerical Study of Flow Past a Rotationally Oscillating Circular Cylinder," *Journal of Fluids and Structure*, Vol. 10, No. 8, 1996, pp. 829–849.

[25]Fujisawa, N., Ikemoto, K., and Nagaya, K., "Vortex Shedding from a Rotary Oscillation Cylinder," *ASME Symposium on Fluid-Structure Interaction, Aeroelasticity, Flow-Induced Vibration and Noise*, AD-Vol. 53-1, American Society of Mechanical Engineers, New York, 1997, pp. 185–190.

[26]Ongoren, A., and Rockwell, D., "Flow Structure from an Oscillating Cylinder. Part 1. Mechanisms of Phase Shift and Recovery in the Near Wake," *Journal of Fluid Mechanics*, Vol. 191, 1988, pp. 197–223.

[27]Ongoren, A., and Rockwell, D., "Flow Structure from an Oscillating Cylinder. Part 2. Mode Competition in the Near Wake," *Journal of Fluid Mechanics*, Vol. 191, 1988, pp. 225–245.

[28]Williamson, C. H. K., and Roshko, A., "Vortex Formation in the Wake of an Oscillating Cylinder," *Journal of Fluids and Structure*, Vol. 2, No. 4, 1988, pp. 355–381.

[29]Lee, T., and Budwig, R., "A Study of the Effect of Aspect Ratio on Vortex Shedding Behind a Circular Cylinder," *Physics of Fluids A*, Vol. 3, No. 2, 1991, pp. 309–315.

[30]Alfredson, P. H., Johansson, A. V., Haristonidis, J. H., and Eekelmann, H., "The Fluctuating Wall-Shear Stress and the Velocity Filed in the Viscous Sublayer," *Physics of Fluids*, Vol. 31, No. 5, 1988, pp. 1026–1033.

[31]Diller, T. E., and Tellionis, D. P., "Time-Resolved Heat Transfer and Skin Friction Measurements in Unsteady Flow," *Advances in Fluid Mechanics Measurements*, edited by M. Gad-el-Hak, Springer–Verlag, New York, 1989, pp. 321–355.

[32]Stack, J. P., Mangalam, S. M., and Berry, S. A., "A Unique Measurement Technique to Study Laminar-Separation Bubble Characteristics on an Airfoil," AIAA Paper 87-1271, 1987.

[33]Dwyer, H. A., and McCroskey, W. J., "Oscillating Flow over a Cylinder at Large Reynolds Number," *Journal of Fluid Mechanics*, Vol. 61, 1973, pp. 753–767.

[34]Roshko, A., "On the Development of Turbulent Wakes from Vortex Streets," NACA Rept. 1191, 1954.

[35]Lorber, P. F., Carta, F. O., and Covino, A. F., "An Oscillating Three-Dimensional Wing Experiment: Compressibility, Sweep Rate, and Geometry Effects on Unsteady Separation and Dynamic Stall," United Technologies, Rept. R92-958325-6, East Hartford, CT, 1992.

J. C. Hermanson
Associate Editor